Advanced Intelligent Discovery

ADVANCED INTELLIGENT DISCOVERY Open Access

RESEARCH ARTICLE OPEN ACCESS

A Computational Approach for Biomimetic Design of Liver-On-A-Chip

Zhenxu Yang[1,2,3] | Qiankun Yin[1,2,3] | Qingxin Liu[1,2] | Zhejun Xu[1,2,3] | Ye Zhang[4] | Christopher Vega-Sánchez[5] | Xiaochen Liu[1,2,3] | Daniele Vigolo[1,3] | Jiao Jiao Li[1,3,4] | Ken-Tye Yong[1,2]

[1]School of Biomedical Engineering, Faculty of Engineering, The University of Sydney, Sydney, Australia | [2]The Biophotonics and Mechanobioengineering Laboratory, Faculty of Engineering, The University of Sydney, Sydney, Australia | [3]The University of Sydney Nano Institute, The University of Sydney, Sydney, Australia | [4]School of Biomedical Engineering, Faculty of Engineering and IT, University of Technology Sydney, Sydney, Australia | [5]School of Electromechanical Engineering, Costa Rica Institute of Technology, Cartago, Costa Rica

Correspondence: Ken-Tye Yong (ken.yong@sydney.edu.au)

Received: 16 June 2025 | **Revised:** 10 December 2025 | **Accepted:** 15 January 2026

Keywords: disease modelling | liver disease | liver-on-a-chip | microfluidics | organ-on-a-chip

ABSTRACT

In this study, we present a biomimetic liver-on-a-chip (LOC) device inspired by the structural organisation of the hepatic acinus and developed through COMSOL Multiphysics simulation. The design incorporates antiparallel perfusion channels and microchannel barriers to mimic nutrient delivery and bile drainage in the liver, while maintaining physiologically relevant low shear stress conditions suitable for hepatocyte culture. A truncated LOC model was first used to explore pressure, shear stress, and concentration distributions, revealing that media perfusion minimally perturbs the cell region while bile flow significantly impacts nutrient diffusion. Full-scale simulations were then performed, demonstrating key discrepancies with the truncated model due to length-dependent diffusion effects, emphasising the importance of simulating full geometries in transport-limited systems. The model was validated experimentally with dye-based flow studies and HepG2 cell culture under dynamic perfusion. Functional validation confirmed that the LOC supports directional solute gradients and cell growth under controlled shear. This integrated in silico–in vitro approach provides a robust framework for the design of organ-on-a-chip systems, reducing development cycles and improving physiological relevance for drug testing and liver disease modelling.

1 | Introduction

The development of organ-on-a-chip (OOC) systems has advanced significantly in recent years, offering a promising alternative to traditional 2D cultures and animal models by better replicating human tissue microenvironments [1–3]. Among these, liver-on-a-chip (LOC) platforms have gained prominence due to their potential in modelling hepatic physiology, drug metabolism, and disease progression [4–6]. However, accurate recapitulation of the hepatic microenvironment remains challenging due to the complex interplay of structural, biochemical, and mechanical cues present in the native liver, particularly within the sinusoidal regions [7–11].

In the native liver microenvironment, hepatocytes are exposed to exceptionally low shear stress, typically less than 1 dyne/cm^2, due to the sinusoidal structure and slow perfusion of blood through the liver acinus [12–14]. Although hepatocyte shear stress can span a broad physiological range, the present study focuses on low shear conditions because these conditions support stable hepatocyte behaviour and avoid the high flow rates that would place unnecessary mechanical and operational demands on the device. This low-shear condition is essential for maintaining hepatocyte polarity, function, and viability, as excessive shear forces can induce cellular damage or phenotypic drift [15]. Reproducing such conditions in vitro has posed a major challenge for LOC development, particularly in balancing adequate nutrient delivery with minimal mechanical stress. Recent studies have addressed this by incorporating microfluidic design

strategies such as porous barriers, staggered channel geometries, and ultrathin membranes to decouple perfusion flow from the cell culture chamber. For example, Gori et al. utilised micro-post arrays to buffer shear forces while enabling directional diffusion of nutrients, and Zhang et al. implemented a dual-layer flow configuration to simulate sinusoidal flow with reduced mechanical load on hepatocytes [16, 17]. These innovations highlight the growing emphasis on fluid dynamic tuning in LOC design, underscoring the need for precise shear regulation to sustain liver-specific functions in vitro.

Computational modelling tools such as COMSOL Multiphysics have emerged as indispensable in the rational design of OOC platforms, enabling predictive simulations of fluid dynamics, mass transport, and shear stress distribution prior to physical fabrication [18–20].

In this study, we present a COMSOL-guided approach to the design of a biomimetic LOC that emulates the antiparallel flow architecture of the liver acinus. The model incorporates microstructured flow barrier configurations to achieve physiologically relevant, low-shear environments essential for maintaining hepatocyte phenotype and function. Using a truncated computational model, we systematically evaluated pressure, shear stress, and concentration distributions across a multichannel microfluidic network. Our simulations confirmed that the LOC design achieves shear stress levels below 1 dyne/cm^2 within the hepatocyte culture region which is well within the range tolerated by liver parenchymal cells while maintaining directional nutrient delivery and waste removal. Importantly, we observed that while the truncated model successfully predicted fluid dynamic behaviour, significant discrepancies in concentration profiles emerged when compared to a full-scale simulation, underscoring the critical impact of length-dependent diffusion processes. This highlights a frequently overlooked limitation in scaled-down models and emphasises the importance of full-geometry simulation for diffusion-dominated systems such as the liver acinus.

The proposed LOC was fabricated and was subsequently validated experimentally. Fluid flow and solute transport behaviours in the fabricated device closely matched the full-scale simulation results. Furthermore, functional testing with HepG2 hepatocytes demonstrated successful cell attachment and growth under dynamic perfusion, confirming the biocompatibility and mechanical appropriateness of the design. Altogether, our study illustrates the power of computational tools in guiding biomimetic microfluidic design and emphasises the need for simulation fidelity when modelling transport-limited biological systems. The combined in silico and in vitro approach reduces trial-and-error iterations and sets a precedent for the rational development of next-generation OOC platforms.

2 | Results and Discussions

2.1 | Design of the Biomimetic LOC Model

A biomimetic LOC device was designed based on the gross anatomical and physiological features of the liver acinus, as schematically illustrated in Figure 1a. The LOC incorporates three primary functional regions: the hepatic artery and portal vein (nutrient supply channels) and the bile duct (waste removal channel), corresponding to the colour-coded channels shown in Figure 1b. In the native liver acinus, hepatocytes are exposed to antiparallel flows of nutrient-rich blood and bile, contributing to their bipolar orientation and zonal functionality [21, 22]. To replicate this arrangement, the LOC was designed with opposing media and bile flow streams to mimic physiological transport gradients and induce region-specific cellular responses. The top and bottom channels of the device represent the nutrient-supplying vasculature, while the central channel serves as the bile drainage pathway. A fully symmetrical layout was adopted to mirror the radial symmetry of the acinus and to ensure balanced flow dynamics. A range of channel widths and heights was explored during the early design stage to understand how geometric changes may influence pressure, shear distribution, and nutrient transport. These exploratory simulations confirmed that the overall behaviour of the system remained consistent across the tested geometries. The antiparallel flow architecture continued to maintain low shear conditions within the cell region, and the transport profiles remained governed by the strong influence of length dependent diffusion along the full channel.

As shown in Figure 1b, additional microchannels were integrated along the outer edges of the device to simulate nutrient diffusion from the media channels into the central cell culture region. The CAD model of a truncated version of the LOC is shown in Figure 1c. To enhance biomimicry and control fluid transfer, the upper and lower media channels were narrowed to increase local pressure and promote directional flow toward the cell chamber. Between the media channels and the central cell region, an array of microchannels (10 μm wide × 30 μm long × 2 μm high) was patterned at 2 μm spacing to facilitate passive diffusion while limiting convective shear. Additionally, another set of microchannels (10 μm × 30 μm × 37 μm) with 10 μm spacing was placed between the cell region and the bile channel to allow efficient removal of metabolic waste while preserving low-shear conditions across the culture area. Although the channel width in the present design is larger than that of hepatic sinusoids, this choice was necessary to ensure reliable fabrication, stable perfusion, and clear imaging, and we acknowledge that narrower geometries may provide improved physiological conditions in future studies.

The design process of our LOC system was guided by a structured computational workflow, as illustrated in Figure 1d. Beginning with computer-aided design (CAD) modelling, we developed a three-dimensional representation of the device's microarchitecture. Subsequently, we employed COMSOL Multiphysics to simulate fluid dynamics and mass transport within the LOC, enabling the calculation of critical parameters such as shear stress, pressure gradients, and solute diffusion profiles. Prior to finalising the current design, multiple iterations were conducted to optimise the microfluidic geometry and operational conditions. This iterative approach was essential, as it allowed for the identification and rectification of potential design shortcomings before fabrication, thereby enhancing the predictive accuracy of the model's performance. Without such computational screening, understanding the device's behaviour and anticipating experimental outcomes would be considerably more challenging.

2.2 | COMSOL Simulation

As shown in Figure 2, pressure distribution was analysed using the truncated LOC model, with the bile channel positioned as the central axis of symmetry. Under equal inlet conditions, the

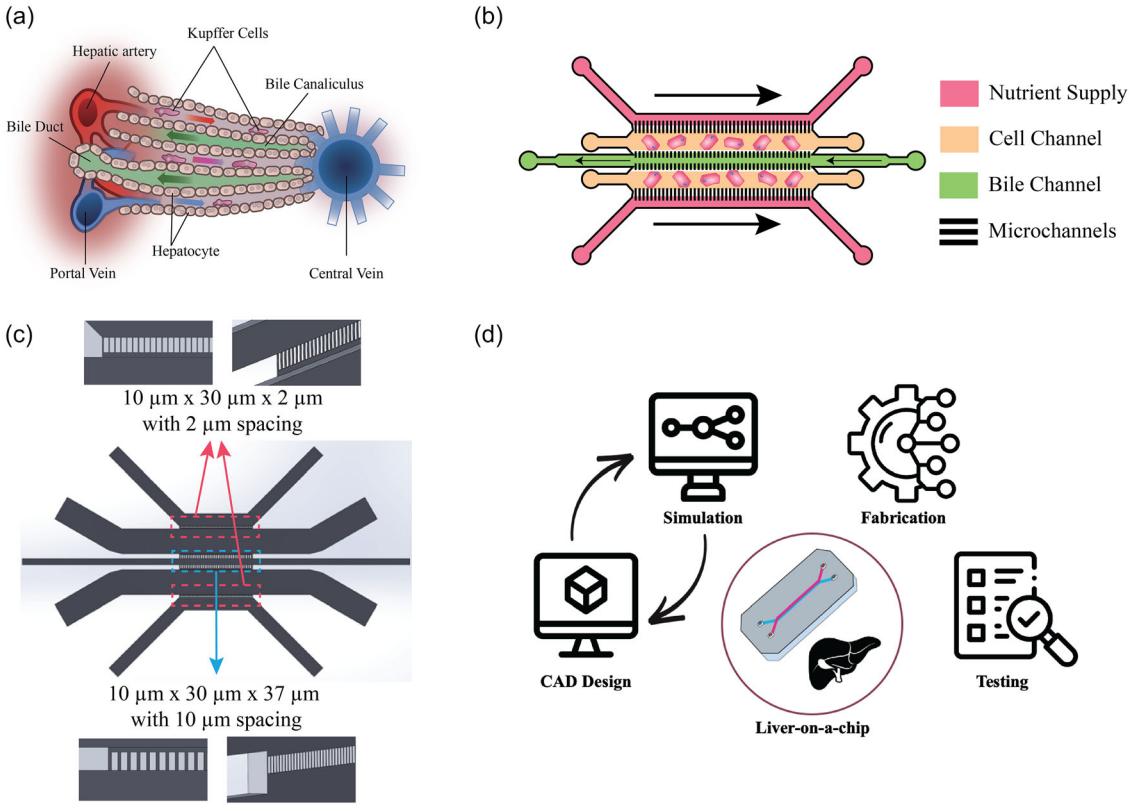

FIGURE 1 | Design concept and development process of the biomimetic LOC system. (a) Schematic of the hepatic acinus, the smallest functional unit of the liver, highlighting zonal blood and bile flow across hepatocytes from the portal vein and hepatic artery toward the central vein. (b) Biomimetic design of the LOC mimicking antiparallel nutrient and bile flow through interconnected channels: pink (nutrient supply), orange (cell culture), and green (bile drainage), separated by microchannel arrays. (c) CAD layout of the LOC showing microchannel arrays between compartments. Nutrient-to-cell channels use shallow microchannels (10 µm × 30 µm × 2 µm, 2 µm spacing), and cell-to-bile channels use deep microchannels (10 µm × 30 µm × 37 µm, 10 µm spacing) to modulate transport while minimising shear. (d) Iterative design workflow for the LOC involving CAD modelling, simulation using COMSOL Multiphysics, microfabrication, and experimental testing to optimise physiological performance.

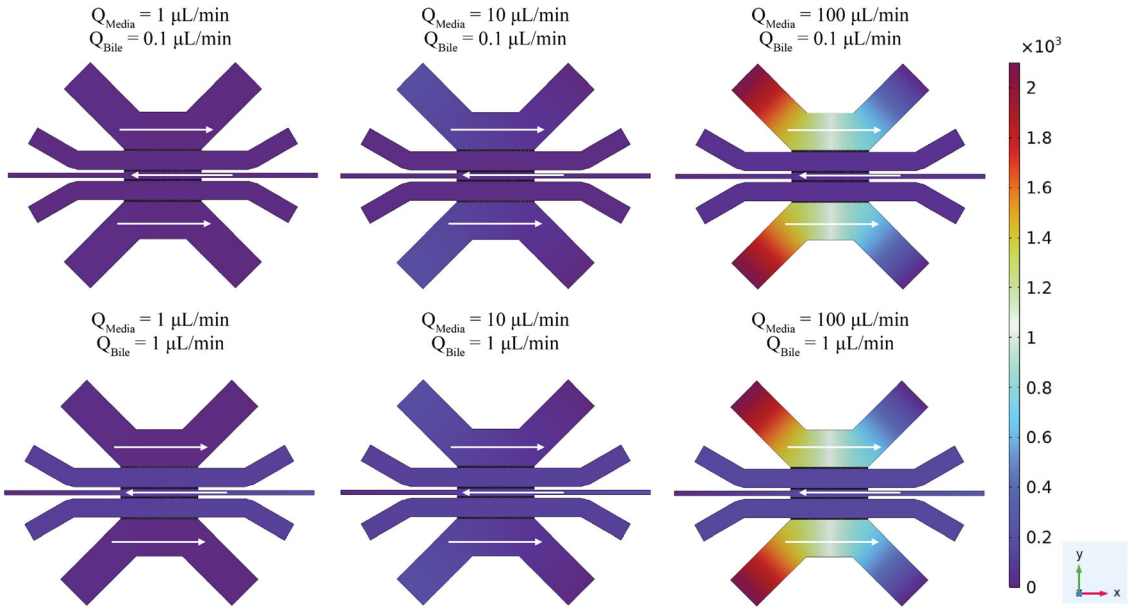

FIGURE 2 | Simulated pressure distribution across the truncated LOC model under varying flow conditions. Pressure contour plots are shown for combinations of media and bile flow rates: 1, 10, and 100 µL/min for media, and 0.1 or 1 µL/min for bile. The bile outlet channel is positioned at the centre of the device, serving as the axis of symmetry.

simulation demonstrated a symmetrical pressure profile across both sides of the chip, indicating balanced flow behaviour. In the top row of Figure 2, the bile flow rate was held constant at 0.1 μL/min, while the media flow rate was increased from 1 to 10 and then to 100 μL/min. Despite this range of media flow rates, the pressure within the central cell channels remained relatively unchanged. This suggests that the media flow has limited influence on the pressure experienced by the cultured cells.

In contrast, the bottom row of Figure 2 presents results with the bile flow rate increased to 1 μL per minute. Under these conditions, the pressure within the cell channels changed more noticeably, indicating that bile flow plays a more direct role in modulating local pressure. This observation is consistent with the device's antiparallel flow configuration, where the bile channel directly interfaces with the cell region through a series of connecting microchannels. Given the parabolic nature of laminar flow in microfluidic systems, fluid velocity is lowest at the channel walls [23]. Therefore, flow from the outer media channels contributes minimal mechanical disturbance to the cells, which is advantageous for preserving cell viability and function.

To gain quantitative insight into the pressure distribution within the microfluidic channels, pressure values were extracted at a vertical height of 18.5 μm, corresponding to the mid-plane of the channel. As illustrated in Figure 3, cutline profiles were plotted at seven distinct *x*-axis positions: −800, −500, −200, 0, 100, 400, and 700 μm, capturing pressure variations along the *y*-axis. These cutlines span all five channels, including the media inlets, the two cell channels, and the bile outlet. The resulting profiles consistently show symmetrical pressure distribution across the device under all tested flow conditions. This symmetry confirms that the model maintains uniform fluid dynamic behaviour between the left and right halves of the chip. Under a fixed bile flow rate, the pressure within the central cell channels remained relatively stable even when media perfusion rates were varied. In contrast, the media channels exhibited more pronounced changes in pressure, particularly at higher flow rates. This observation further supports the idea that the cell region is shielded from large mechanical disturbances, which is important for maintaining cell viability and mimicking physiological shear environments. These findings confirm that the LOC design successfully maintains a low-shear environment while allowing directional flow. The increase in bile flow introduces more significant pressure shifts across the cell area, which may be useful for tuning solute gradients or simulating waste clearance dynamics in future applications.

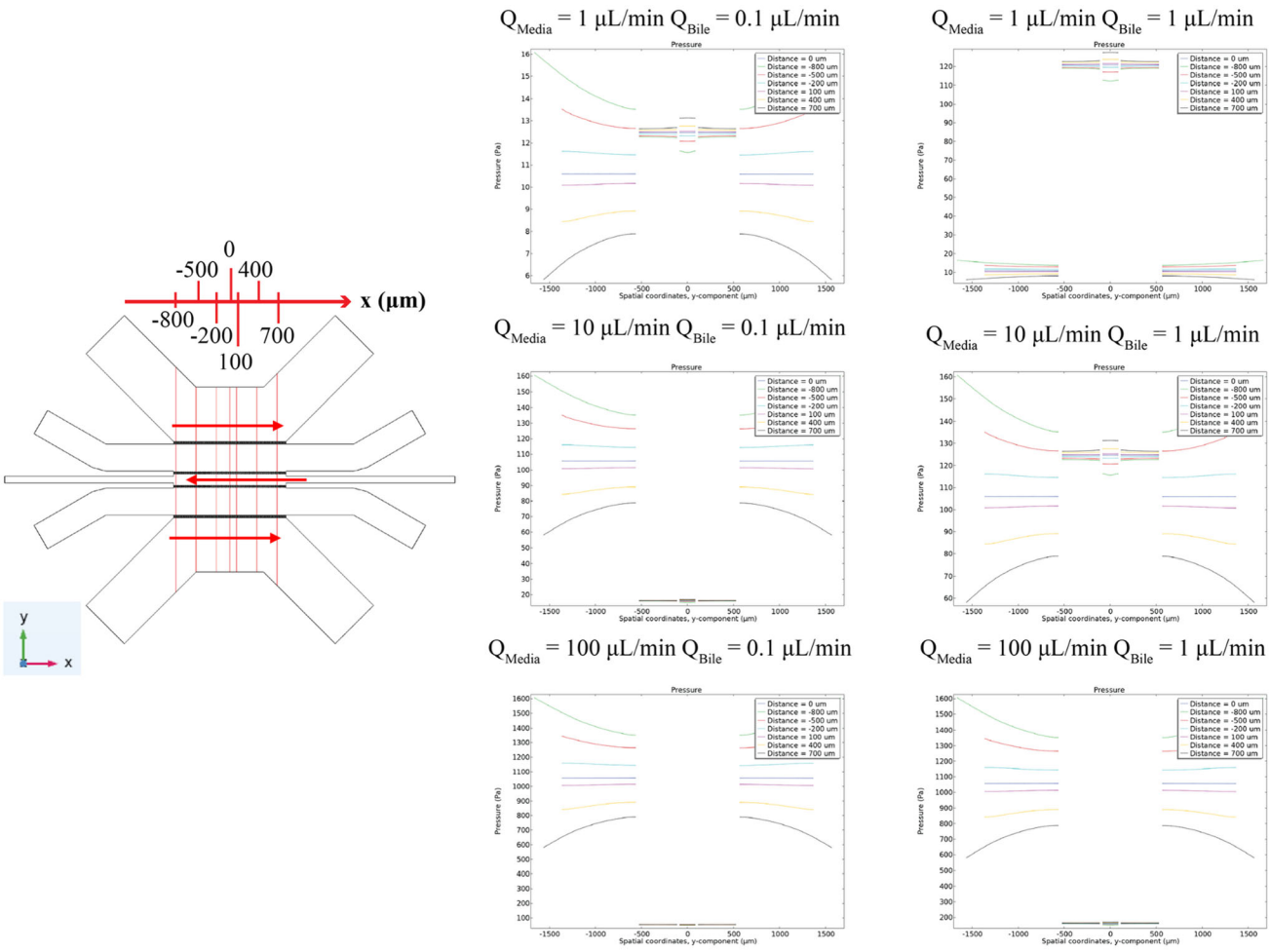

FIGURE 3 | Quantitative pressure profiles along the *y*-axis at various *x*-positions in the truncated liver-on-a-chip (LOC) model. Pressure was extracted at a channel height of 18.5 μm (mid-plane) along the *y*-axis at seven *x*-positions: –800, –500, –200, 0, 100, 400, and 700 μm, as indicated by red lines in the schematic (left). Line plots (right) show pressure distributions across five flow conditions: combinations of media flow rates (1, 10, and 100 μL/min) and bile flow rates (0.1 and 1 μL/min).

Shear stress is a critical mechanical cue in organ-on-a-chip systems, as it influences cell morphology, function, and viability. Typical OOC platforms are designed to deliver shear stress ranging from 1 dyne/cm^2 to just under 100 dyne/cm^2, which corresponds to ≈1–100 dPa [24]. These values are representative of physiological levels encountered in vascular systems. However, hepatocytes are known to experience much lower shear stress in vivo, generally below 1 dyne/cm^2 [4, 15]. Therefore, achieving low shear stress is essential for accurately mimicking the hepatic microenvironment in LOC systems. In our LOC design, shear stress distributions were evaluated under various flow conditions to ensure that the mechanical microenvironment remains within physiologically relevant levels. Similar to pressure analysis, we observed that higher media flow rates led to increased shear stress in the perfusion channels. However, the effect on the central cell channels was minimal. This was a direct result of the device architecture, particularly the low-height microchannel barriers that restrict convective flow into the cell chambers. These barriers reduce direct shear transmission while allowing molecular diffusion, thus protecting cells from excessive mechanical stimulation.

Shear stress was analysed at two vertical positions, one at the bottom of the channel (0 μm) and another at the mid-plane (18.5 μm). These positions were chosen to represent wall-level and mid-channel conditions, respectively. As shown in Figure 4, shear stress profiles at these two positions revealed opposite trends, which is consistent with previously reported simulations in microfluidic systems. Shear stress is highest near the walls due to the no-slip boundary condition and gradually decreases toward the centre of the channel. To focus the analysis on the cell region, shear stress profiles from the media perfusion channels were excluded from Figure 4. The results clearly indicate that the highest shear stress in the cell channels occurred when media and bile flow rates were set at 100 μL/min and 1 μL/min, respectively. Under this condition, the peak shear stress within the cell region reached ≈0.7 dyne/cm^2 or 0.7 dPa, which remains within the physiological range for hepatocytes. Changes in bile flow had a more substantial impact on shear stress within the cell channels compared to changes in media flow. This suggests that the bile outlet channel plays a key role in modulating mechanical forces experienced by cells. The narrow 2 μm high microchannels connecting the media and cell channels functioned effectively as shear dampers. These structures also serve a dual purpose by preventing unwanted cell migration into the nutrient channels while still supporting passive nutrient diffusion.

Next, we evaluated the concentration distribution within the device, which is another critical parameter that influences nutrient availability and cellular response. In our model, nutrient transport into the central cell channels is primarily driven by diffusion from the upper and lower media supply channels, since active flow across the microchannel barriers is minimal. To visualise solute distribution, a constant concentration of 1 μL/mL was applied at both media inlets, while the bile outlet channel was supplied with a concentration of 0 μL/mL. This configuration simulates the effect of using the bile channel as a purging outlet. As shown in Figure 5, the presence of a zero-concentration sink

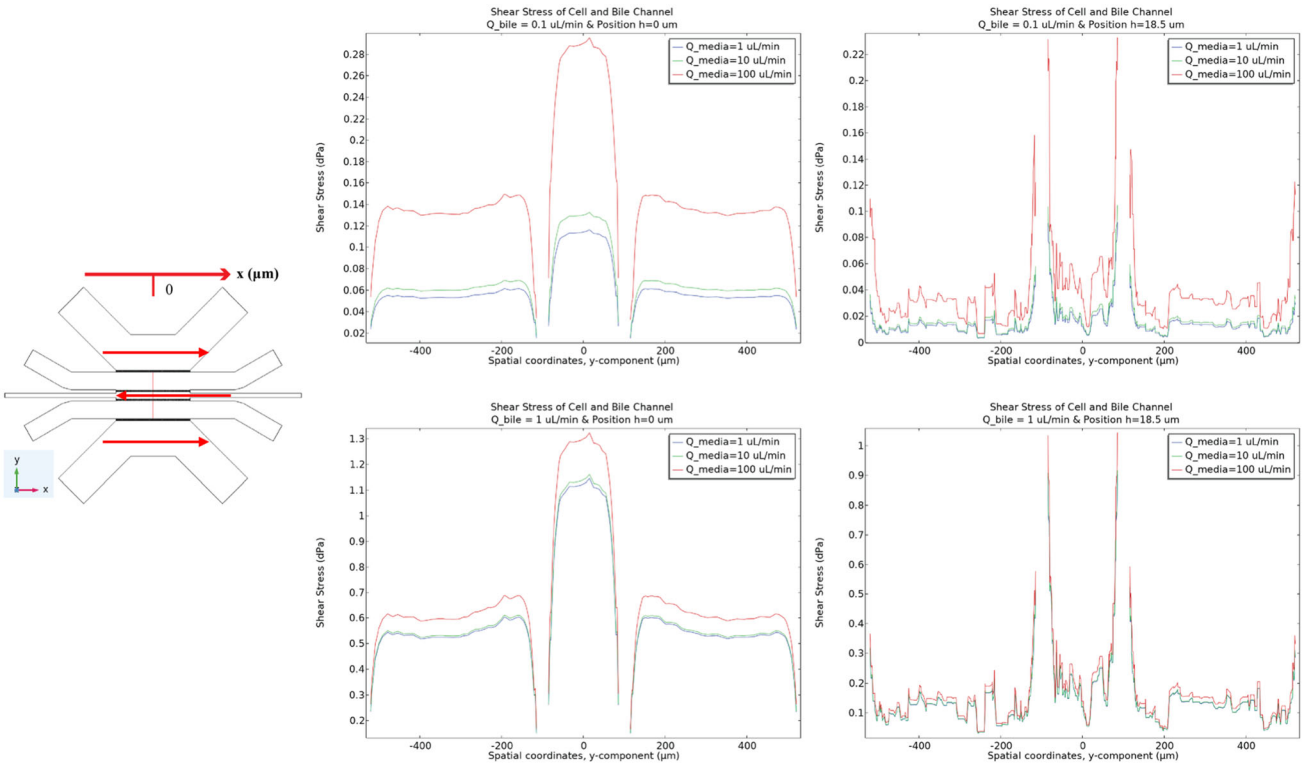

FIGURE 4 | Shear stress profiles across the truncated LOC model under varying flow conditions. Shear stress was computed along the *y*-axis at two vertical positions: (left) 0 μm (channel wall) and (right) 18.5 μm (channel mid-height). Each row represents a different bile flow rate: 0.1 μL/min (top) and 1 μL/min (bottom), with media flow rates of 1, 10, and 100 μL/min. Plots show shear stress distribution within the central region of the device. As expected, shear stress is highest near the wall (0 μm) and lowest at mid-channel height (18.5 μm), reflecting the parabolic velocity profile of laminar flow.

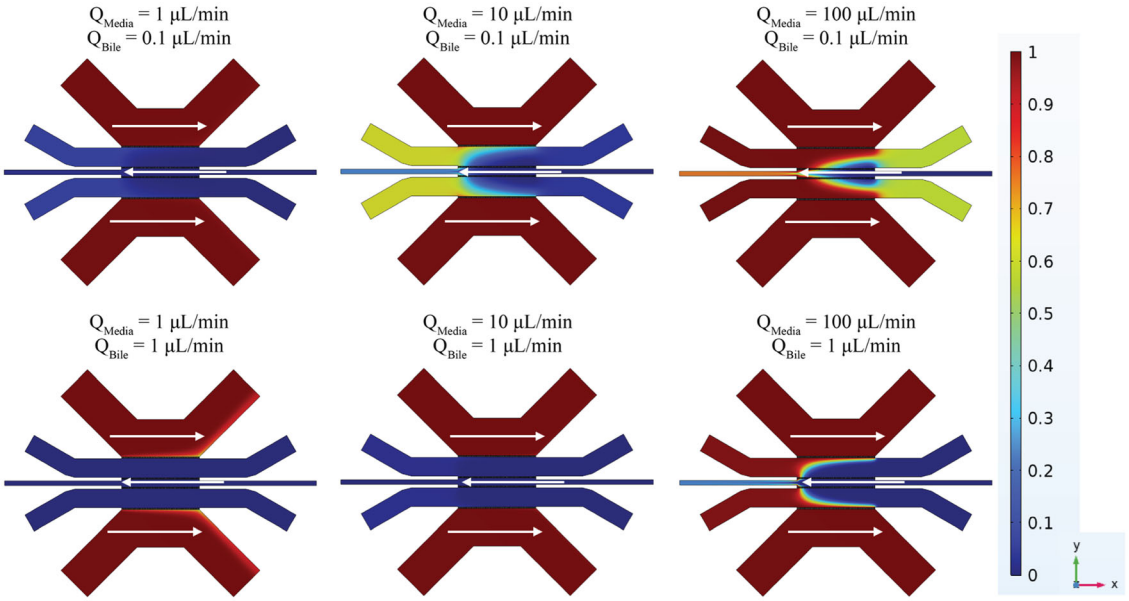

FIGURE 5 | Simulated concentration distribution across the truncated LOC model under various media and bile flow rates. Concentration contours are shown for combinations of media flow rates (1, 10, and 100 µL/min) and bile flow rates (0.1 and 1 µL/min), with the nutrient concentration set to 1 µmol/mL at the media inlets and 0 µmol/mL at the bile outlet. At low media flow (1 µL/min), nutrient diffusion into the cell channel is limited, especially when bile flow is high. Increasing the media flow rate improves concentration penetration into the cell channel, with optimal gradients observed at 10 µL/min media and 0.1 µL/min bile flow. At the highest media flow (100 µL/min), nutrient concentration approaches uniform distribution across the cell chamber.

in the bile channel creates a concentration gradient across the cell channels. Interestingly, this configuration also allows modulation of nutrient distribution by simply tunning bile flow rate. Even with varying bile flow conditions, the overall concentration profiles within the cell regions remained symmetrical, consistent with the device's structural symmetry.

Different combinations of media and bile flow rates significantly influence the nutrient concentration profiles within the cell channels. In the truncated model, when the media flow rate was set to 1 µL/min and the bile flow rate to 0.1 µL/min, nutrient delivery to the cell channels was minimal. As shown in Figure 6, the maximum concentration achieved under this condition was ≈0.075 µmol/mL. When the bile flow rate was increased to 1 µL/min, the concentration dropped further, approaching zero, indicating that the purging effect from the bile outlet suppressed nutrient diffusion into the cell region.

Increasing the media flow rate to 10 µL/min significantly improved nutrient delivery. Under a bile flow rate of 0.1 µL/min, the maximum concentration in the cell channel reached ≈0.7 µmol/mL. Further, raising the bile flow to 1 µL/min again reduced the peak concentration to around 0.03 µmol/mL, reaffirming the strong influence of bile flow on concentration gradients. At the highest media flow rate of 100 µL/min, the concentration distribution became more uniform across the cell channel. Under both bile flow conditions, the maximum concentration approached that of the media inlet at 1 µmol/mL. With the bile flow held at 0.1 µL/min, the nutrient-rich region expanded, maintaining a broader area of high concentration within the cell channel. In contrast, when bile flow was increased to 1 µL/min, the gradient became steeper, but the peak value remained high due to the strong driving force from the media inlets.

These results demonstrate that the proposed LOC device can maintain uniform and tuneable concentration gradients across the cell culture region, which is essential for applications requiring controlled solute exposure, such as drug diffusion studies, metabolic zonation, and gradient-guided cell behaviour analysis. The ability to establish these gradients without introducing significant shear or convective flow highlights the effectiveness of the diffusion-driven architecture in replicating physiological transport mechanisms. The design allows different experimental conditions to be applied while keeping flow dynamics consistent across the device. With pressure remaining constant, solute concentration becomes the primary variable, enabling the creation of internal control groups within a single platform. Furthermore, the truncated model has been shown to accurately reproduce both mechanical and mass transport conditions suitable for LOC systems, supporting physiologically relevant nutrient levels and concentration gradients required for studying diffusion-dependent liver functions.

To evaluate the robustness and scalability of the design, a full-scale CAD model of the LOC was developed and simulated using COMSOL Multiphysics. While the full-scale simulation required significantly greater computational resources, the optimised three-dimensional model allowed successful completion of the analysis. Encouragingly, the full-scale results were consistent with those obtained from the truncated model, thereby validating the reliability and scalability of the design. As shown in Figure 7, the pressure distribution remained symmetrical when using the bile outlet channel as the central axis. Under identical inlet conditions, the full-scale model reproduced the balanced pressure profiles observed in the truncated version. When the bile flow rate was fixed at 0.1 µL/min, and the media perfusion rate was varied across 1, 10, and 100 µL/min, the pressure within

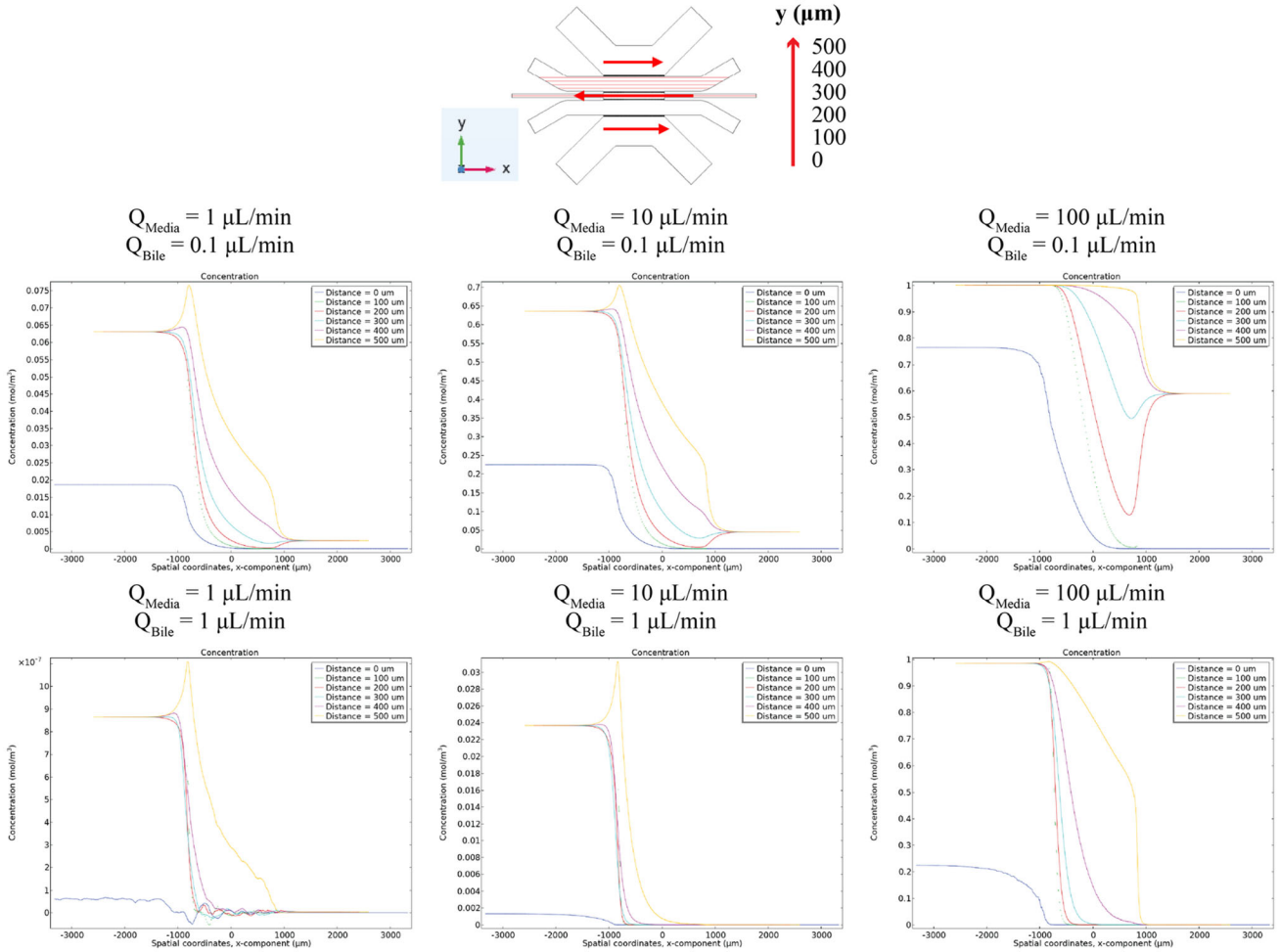

FIGURE 6 | Line profile analysis of concentration distribution across the *x*-axis at multiple *y*-positions in the truncated LOC model. Concentration profiles were extracted along the *x*-direction at vertical distances of 0, 100, 200, 300, 400, and 500 μm from the base of the cell culture channel. Each plot represents a specific combination of media (1, 10, or 100 μL/min) and bile (0.1 or 1 μL/min) flow rates. At low media flow (1 μL/min), concentration penetration into the cell region is minimal, particularly when bile flow is elevated, reflecting a strong downstream sink effect. As media flow increases, nutrient delivery improves, with the most uniform and physiologically relevant gradient observed at 10 μL/min media and 0.1 μL/min bile. At 100 μL/min media flow, concentration profiles show near saturation across the region, with steeper gradients observed under higher bile flow.

the cell channels remained relatively unaffected. This confirms that nutrient flow from the media channels imposes minimal pressure changes on the cell region. In contrast, increasing the bile flow rate to 1 μL/min introduced more noticeable pressure shifts, particularly within the central channels. These results align with prior findings and further support the conclusion that bile flow plays a more significant role in modulating the fluid dynamics near the hepatocyte culture area. The full-scale simulation confirms that the LOC design can maintain controlled and symmetric flow conditions across a range of flow rates, reinforcing its suitability for physiological modelling and experimental consistency.

To further quantify pressure distribution in the full-scale model, pressure values were extracted at a height of 18.5 μm, corresponding to the mid-plane of the channel. As illustrated in Figure 8, line cut profiles were plotted along the *y*-axis at multiple *x*-positions: −800, −500, −200, 0, 100, 400, and 700 μm. These cutlines span across all five channels, capturing pressure variations under different flow conditions. Across all tested flow combinations, the pressure profiles displayed clear symmetry, indicating that the full-scale model maintains balanced fluid dynamics along the central axis. Similar to the truncated model, changes in media perfusion rates had limited influence on the pressure within the central cell channels when the bile flow rate was held constant. In contrast, varying the bile flow rate introduced more noticeable effects, confirming its dominant role in modulating internal pressure conditions. Compared to the truncated model, the full-scale simulation exhibited more stable and uniform pressure distributions along the channel length. This enhanced stability is likely due to the extended geometry, which provides sufficient distance for the flow to fully develop. Additionally, while the absolute pressure magnitudes increased significantly in the full-scale model, especially at higher flow rates, the overall trends remained consistent with those observed in the truncated version.

The mechanical microenvironment in the full-scale LOC model was evaluated, where shear stress distributions were analysed at two vertical positions: 0 μm, corresponding to the channel wall, and 18.5 μm, corresponding to the mid-plane of the channel. As shown in Figure 9, shear stress values were plotted along the

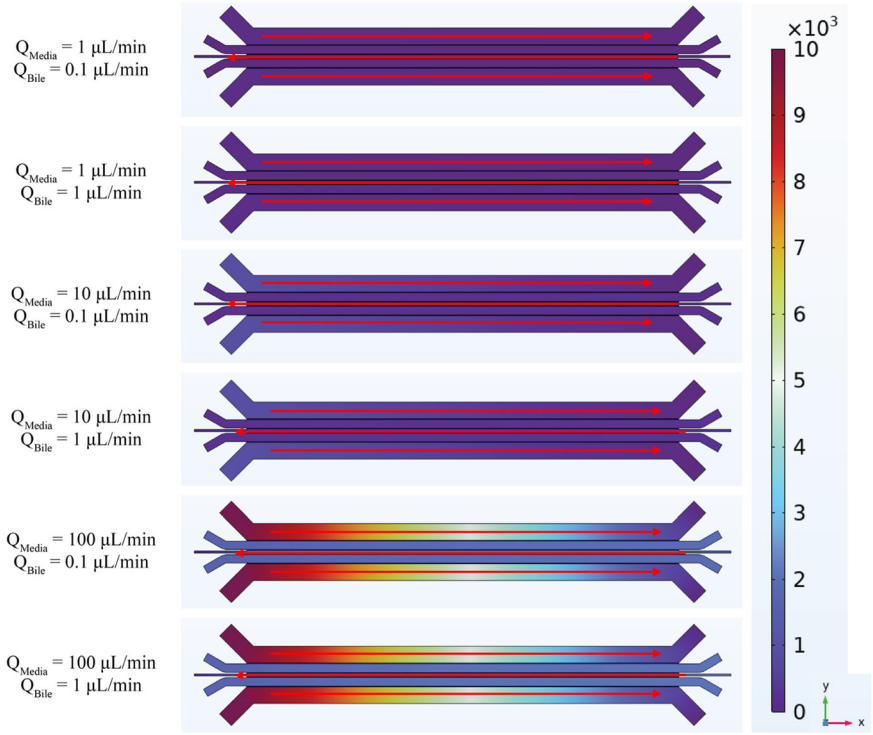

FIGURE 7 | Simulated pressure distribution in the full-scale LOC model under various flow conditions. Pressure contour maps are shown for media flow rates of 1, 10, and 100 µL/min combined with bile flow rates of 0.1 and 1 µL/min. The full-length geometry enables observation of pressure stabilisation along the extended microchannel. As seen in the figure, pressure symmetry is maintained across the bile outlet axis, confirming balanced flow conditions in the full-scale design. While increasing media flow results in elevated overall pressure within the perfusion channels, the pressure within the central cell region remains relatively stable. Bile flow, on the other hand, has a more pronounced impact on the cell region's pressure profile.

y-axis for a central *x*-plane under various combinations of media and bile flow rates. The results exhibit consistent trends observed in the truncated model, with clear differences in magnitude due to the extended geometry of the full-scale device.

At the channel wall (position = 0 µm), shear stress reached its maximum across all tested conditions, which aligns with the expected no-slip boundary behaviour in microfluidic flows. The highest shear stress values were observed at the media flow rate of 100 µL/min, with values exceeding 1.3 dPa when the bile flow rate was set at 0.1 µL/min, and approaching 1.8 dPa at a bile flow rate of 1 µL/min. At the mid-channel height (position = 18.5 µm), shear stress magnitudes decreased significantly in all cases, consistent with the parabolic flow profile characteristic of laminar systems. Although shear stress fluctuations were more irregular at this position, the overall magnitudes remained within physiologically tolerable limits for hepatocyte culture. Importantly, the results reinforce the shielding effect of the microchannel design, which effectively limits direct shearing within the cell culture regions.

Together, these findings confirm that the full-scale model successfully maintains a low-shear environment across a range of perfusion conditions. The device can replicate physiologically relevant mechanical cues without exposing cells to excessive wall shear stress, thereby supporting its application for hepatocyte culture and broader LOC studies. The trends are consistent with the truncated model but provide further confidence thanks to the improved spatial resolution and stability offered by the extended geometry.

Interestingly, the full-scale model revealed clear differences in concentration distribution (Figure 10) compared to the truncated model (Figure 5), highlighting the importance of device length in diffusion-driven transport. In the truncated model, lower media flow rates failed to deliver sufficient nutrients to the cell region. However, in the full-scale simulation, even at a media flow rate of 1 µL/min and a bile flow rate of 0.1 µL/min, the cell channel was able to sustain a concentration exceeding 0.7 µmol/mL. This improvement can be attributed to the extended channel length, which allowed more time and distance for solute diffusion to establish a gradient across the device.

Despite this benefit, increasing the bile flow rate to 1 µL/min eliminated nutrient availability in the cell region, mirroring the outcomes of the truncated model. This confirms that bile flow acts as a dominant sink, capable of overriding diffusion from the media channels when elevated. Among all tested conditions, the combination of 10 µL/min media flow and 0.1 µL/min bile flow produced the most physiologically representative profile. Under this setting, the concentration across the cell channel exhibited a smooth decline from left to right. This transition effectively reproduces the nutrient gradient from the portal triad to the central vein in the native liver acinus. Such a gradient is ideal for studies involving cell spreading, metabolic zonation, and position-specific cell behaviour within the liver-on-a-chip system.

To evaluate nutrient distribution in greater detail, spatial concentration profiles were extracted along the *x*-axis at several *y*-positions across the cell region in the full-scale model. As shown in Figure 11, the profiles were generated at vertical distances of 0, 100, 200, 300, 400, and 500 µm from the channel floor to capture concentration variations through the cell culture zone under different combinations of media and bile flow rates.

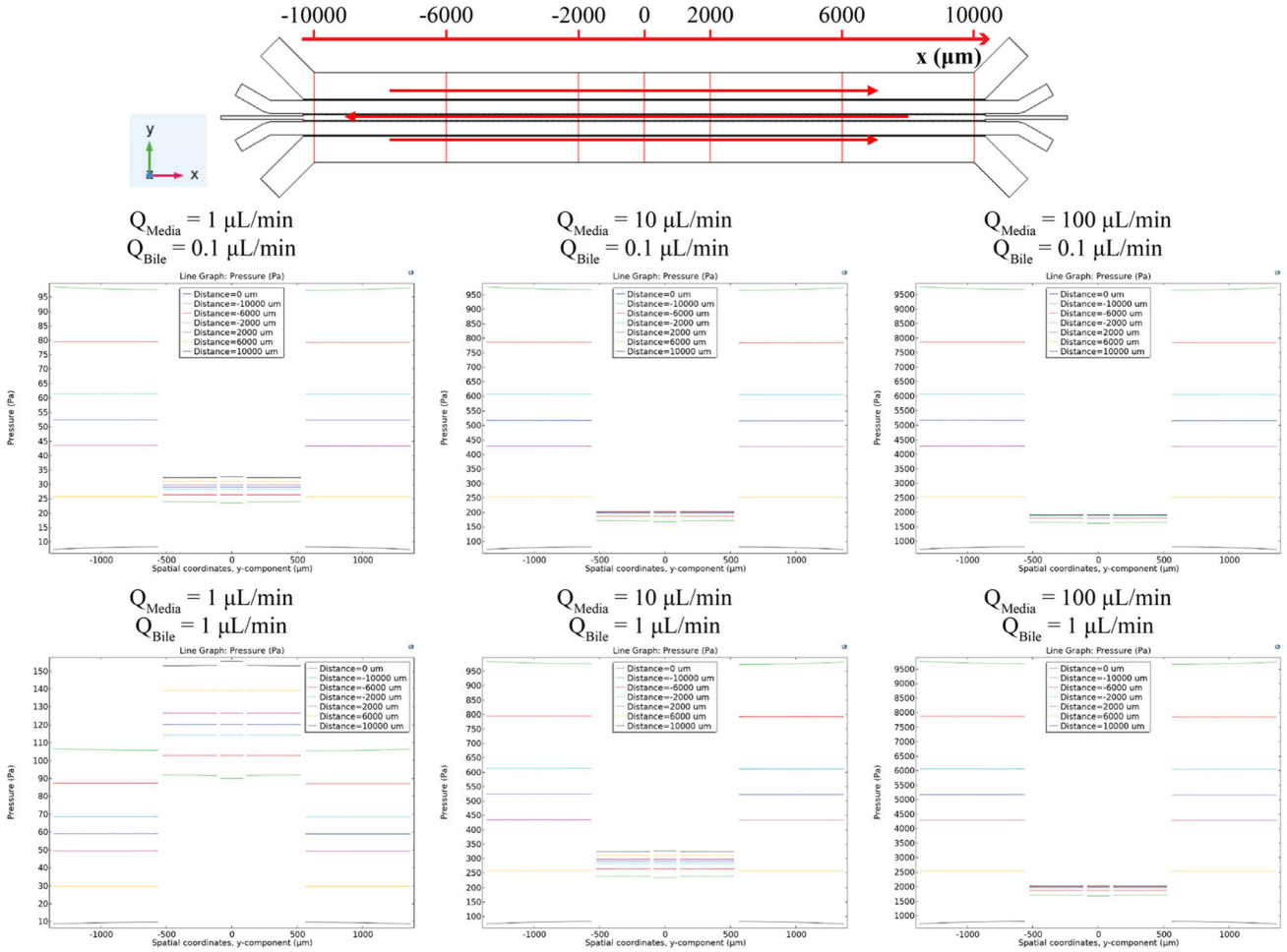

FIGURE 8 | Quantitative pressure profiles along the *y*-axis at multiple *x*-positions in the full-scale LOC model. Pressure was extracted at a height of 18.5 μm (channel mid-plane) along the *y*-direction at *x*-positions of −10 000, −6000, −2000, 0, 2000, 6000, and 10 000 μm, as indicated in the schematic (top left). Each plot represents a specific combination of media (1, 10, or 100 μL/min) and bile (0.1 or 1 μL/min) flow rates.

At lower media flow rates (1 μL/min) and low bile flow (0.1 μL/min), the concentration gradually decreased along the *x*-axis with increasing distance from the inlet, consistent with diffusion-dominated transport. This setup allowed nutrient diffusion through the full length of the chip, with a moderate gradient spanning from inlet to outlet. However, when the bile flow rate was increased to 1 μL/min under the same media flow, the concentration dropped sharply near the inlet and fell to near-zero levels throughout most of the device length. This suggests that the bile outlet exerted a dominant sink effect, pulling solutes away from the cell region before they could distribute effectively.

At higher media flow rates of 10 μL/min and a bile flow of 0.1 μL/min, the gradient became more stable and linear, extending from the inlet to the outlet with distinguishable layering at different *y*-positions. This configuration effectively established a smooth and interpretable concentration gradient across the cell region, suitable for experimental models that aim to study cell behaviour across nutrient transitions. Conversely, with a bile flow rate of 1 μL/min, the profiles became compressed, and nutrient depletion was observed earlier along the *x*-axis, particularly at positions closer to the channel base.

With the highest media flow rate of 100 μL/min, the effects became more pronounced. Under low bile flow, concentration remained near saturation throughout most of the channel, but under high bile flow, the gradient was skewed and heavily influenced by competitive flushing effects. In this case, nutrient levels dropped quickly after the inlet, particularly near the lower regions of the culture channel, suggesting stratification and reduced distribution depth.

Overall, these full-scale profiles confirm that while higher media flow enhances nutrient delivery, elevated bile flow significantly disrupts uniform solute distribution. The results emphasise the need to finely tune bile outlet flow to avoid excessive dilution and to preserve functional concentration gradients. The extended geometry of the full-scale model allowed for these effects to be clearly resolved and quantified, providing valuable insight into flow-mediated mass transport dynamics within the LOC system.

2.3 | Validation of the LOC

The master silicon mould was fabricated by the ANFF-SA node and treated with hexamethyldisilazane (HMDS) to improve the release properties for soft lithography using polydimethylsiloxane (PDMS). Following fabrication, the device was validated by comparing in silico concentration profiles with experimental dye flow observations. To visualise solute transport, blue and

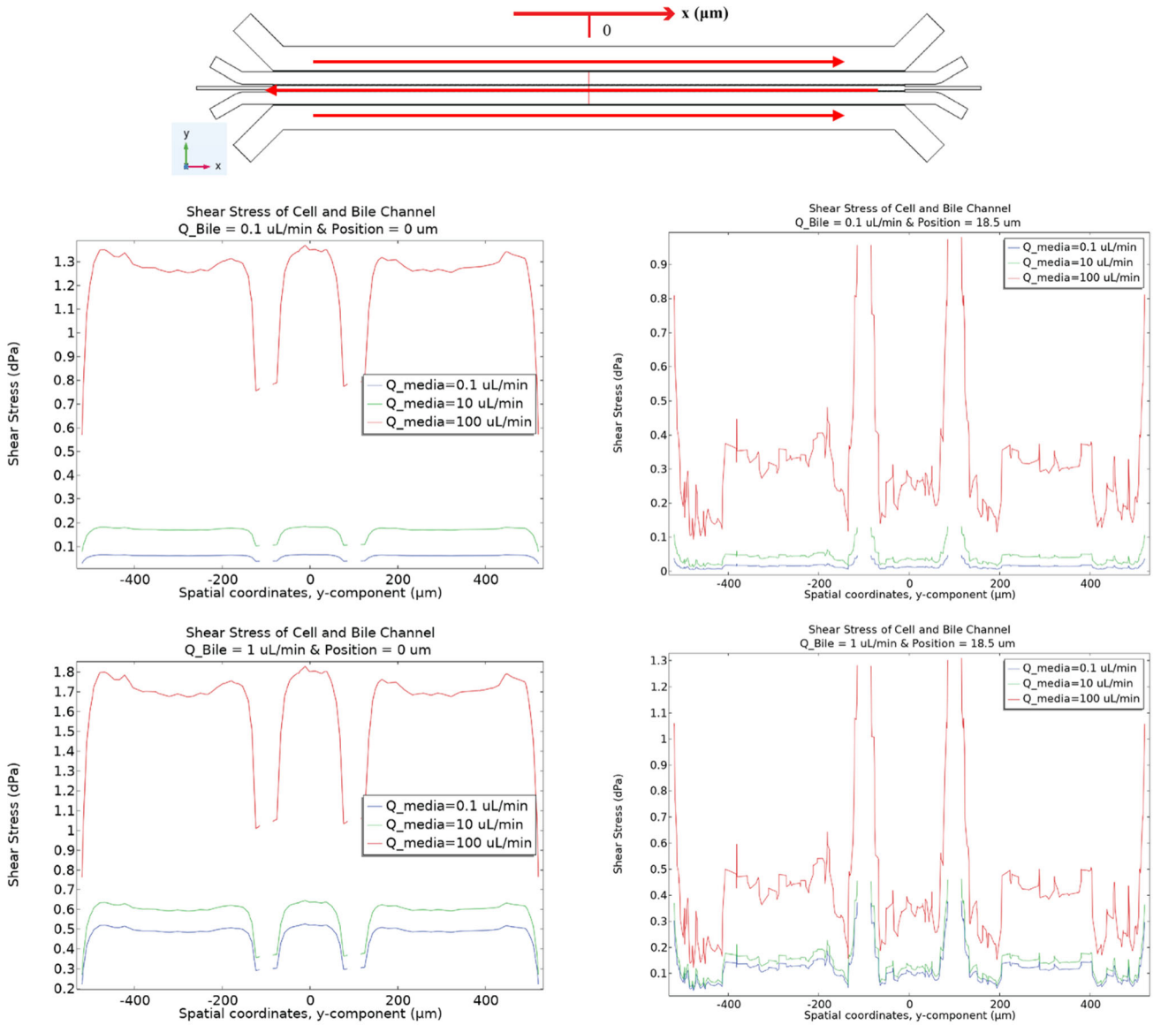

FIGURE 9 | Shear stress profiles across the full-scale LOC model under various flow conditions. Shear stress was computed along the *y*-axis at two vertical positions: 0 μm (channel wall) and 18.5 μm (channel mid-plane), as shown in the schematic (top left). Each row of plots corresponds to bile flow rates of 0.1 μL/min (top) and 1 μL/min (bottom), while each curve represents a different media flow rate (1, 10, and 100 μL/min). At the wall (0 μm), shear stress peaked near channel boundaries and increased with both bile and media flow rates. At the mid-plane (18.5 μm), shear stress was lower overall but showed localised fluctuations depending on flow configuration.

yellow food dyes were introduced into the media inlets, simulating nutrient diffusion across the central cell channel. As shown in Figure 12a–e, the experimentally observed colour distribution closely matched the simulated results obtained under a media flow rate of 100 μL/min and a bile flow rate of 1 μL/min. This agreement supports the robustness of the computational approach. It is important to note that this agreement in concentration profile was only observed when comparing to the full-scale simulation, rather than the truncated model. This highlights the critical role of length-dependent diffusion dynamics, which are governed by Fick's Second Law of Diffusion. According to Fick's Law, the rate of mass transport is proportional to the concentration gradient and the diffusion coefficient, but the spatial extent over which diffusion occurs is directly influenced by both the time and characteristic length scale. Specifically, the relationship $L \propto \sqrt{Dt}$, where D is the diffusion coefficient, L is distance, and t is time, implies that in shorter systems (like the truncated model), solute diffusion is artificially constrained, leading to underestimation of nutrient transport [25, 26]. Thus, full-scale modelling is necessary to capture physiologically relevant concentration gradients in diffusion-limited organ-on-a-chip systems.

The LOC architecture also maintained low shear stress levels, consistent with physiological liver sinusoidal conditions. As previously discussed, the microchannel design was optimised to ensure minimal mechanical disruption to cultured cells. For in vitro studies, a media flow rate of 10 μL/min and a bile flow rate of 0.1 μL/min were applied to achieve a shear stress of ≈0.2 dPa in the cell channel region. Figure 12f illustrates the experimental setup, which incorporated an Elveflow OB1 pressure controller for precise media perfusion, and a syringe pump

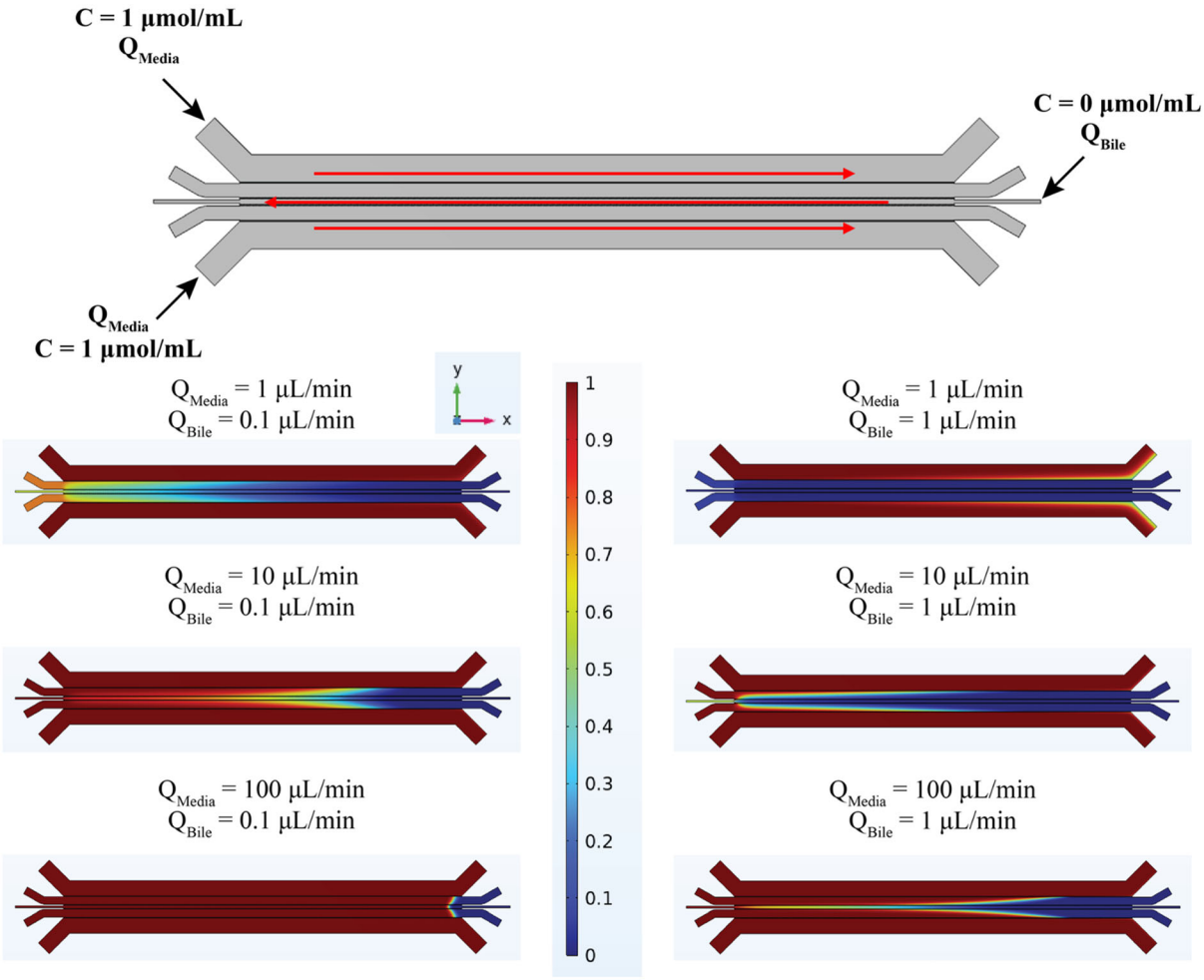

FIGURE 10 | Simulated concentration distribution in the full-scale LOC model under varying media and bile flow rates. Concentration contours are shown for three media flow rates (1, 10, and 100 µL/min) and two bile flow rates (0.1 and 1 µL/min), with nutrient concentration set at 1 µmol/mL at the media inlets and 0 µmol/mL at the bile outlet.

to regulate bile purge. The outlet flows from all liquid channels were directed into a shared collection tube to maintain pressure balance and simplify downstream sample analysis.

To assess the biological performance of the chip, HepG2 cells were cultured over a 2-day period under continuous perfusion. Figure 12g presents microscopic images from four longitudinal regions of the cell channel across Day 0, Day 1, and Day 2. Initially, cells were randomly distributed across the channel surface. By Day 1, an increase in cell density was observed, with asymmetry noted between the upper and lower regions of the chip. Specifically, the left side of the chip exhibited higher cell coverage in the upper channel, while the right side showed a greater concentration in the lower channel. By Day 2, cell growth continued in all regions, with region 4 showing unexpectedly high cell density. Interestingly, dense cell accumulation was also observed in the bile outlet channel. This may have obstructed media flow and altered local nutrient delivery, thereby contributing to the abnormal growth distribution. Despite this deviation, the overall results confirm that the LOC supports hepatocyte proliferation under both diffusive transport and biomimetic shear stress conditions. The platform demonstrates potential for future studies in liver physiology, gradient-based cell responses, and drug metabolism modelling in a controlled microfluidic environment.

2.4 | Limitations and Future Perspectives

Our present design uses channels that are wider than hepatic sinusoids, which limits the ability of the device to fully reproduce the structural environment experienced by hepatocytes in vivo. Wider channels were selected to support reliable fabrication, stable perfusion, and clear optical access, but this choice may reduce the formation of certain physiological features, such as polarity cues and bile canaliculi structures. This represents an important limitation of the current platform. Future work will explore methods to reduce channel width and introduce structures that more closely reflect the native sinusoidal environment. This may include revised fabrication strategies that allow narrower channels with consistent performance, as well as the introduction of endothelial cells that provide additional physical and biochemical guidance. These directions will improve the physiological relevance of the device and strengthen its suitability for advanced biological investigations.

Our study focuses on the development and validation of a biomimetic antiparallel flow architecture for a LOC system. The study relies mainly on computational analysis supported by qualitative tracer experiments. Although the tracer study confirms the expected flow behaviour, the work does not include quantitative measurements of velocity fields within the device. This is

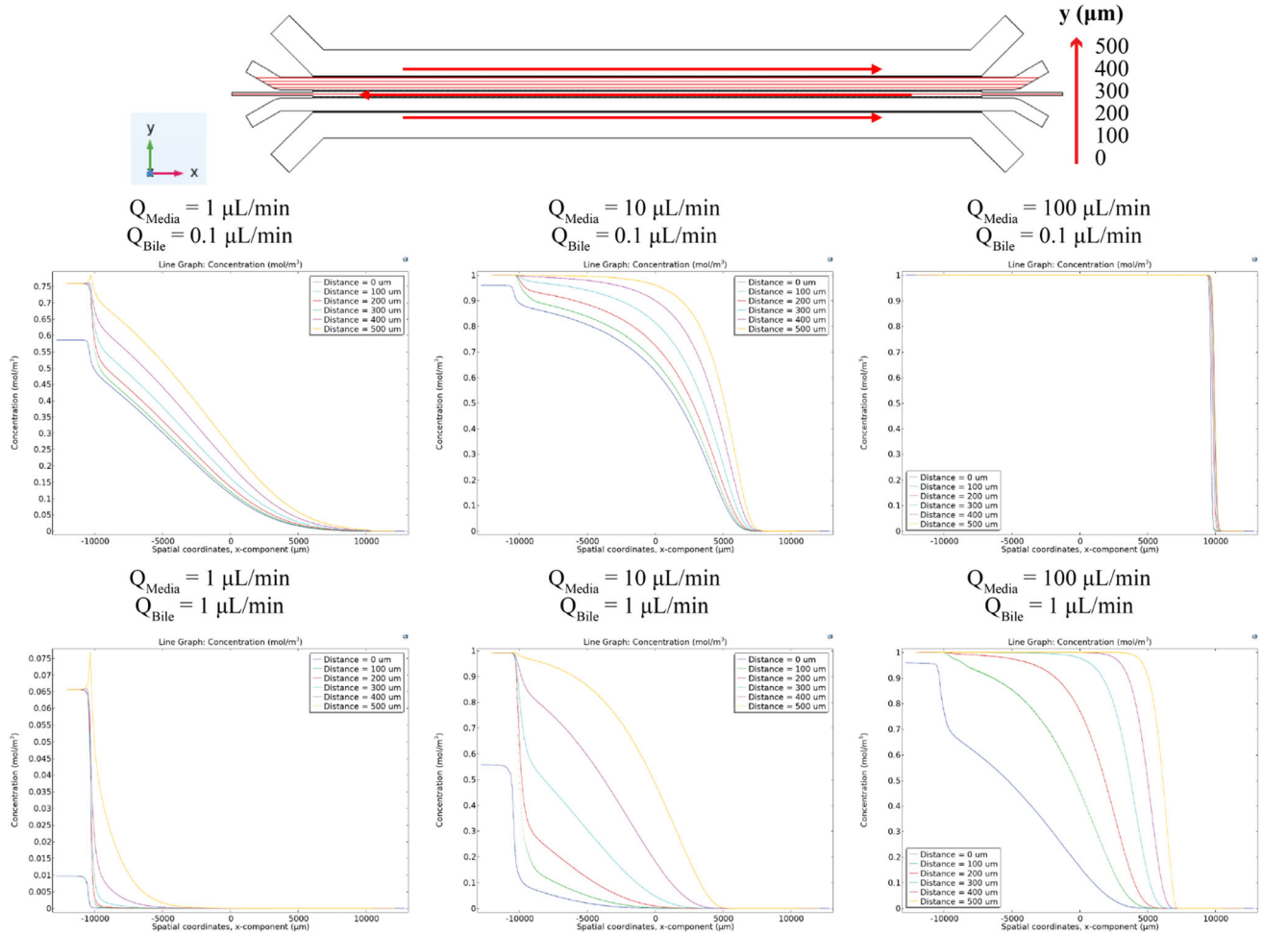

FIGURE 11 | Line profile analysis of concentration gradients along the *x*-direction in the full-scale LOC model. Concentration values were extracted along horizontal lines at multiple *y*-positions (−8000, −5000, −2000, 0, 2000, 5000, and 8000 μm) from the central bile axis to assess solute distribution across the length of the device. Profiles are shown for combinations of media flow rates (1, 10, and 100 μL/min) and bile flow rates (0.1 and 1 μL/min). The full-scale model revealed smoother and more physiologically relevant gradients compared to the truncated model, particularly at 10 μL/min media and 0.1 μL/min bile flow, which yielded a continuous decrease in concentration across the cell chamber. Elevated bile flow (1 μL/min) markedly reduced concentration levels due to enhanced purging, while high media flow (100 μL/min) led to uniform concentration distribution with minimal gradient.

an important limitation of the present design stage because experimental flow mapping would provide direct confirmation of the simulated pressure and velocity values and would strengthen the overall validation of the model. Future studies will therefore incorporate detailed measurements of fluid behaviour in the full-length channel system. This will include the use of particle-based flow tracking or related imaging methods to obtain velocity field data along the perfusion pathway. These measurements will allow direct comparison with the computational model and will support refinement of boundary conditions and simulation parameters. The addition of these studies will improve confidence in the transport analysis and will guide further optimisation of the LOC platform for subsequent biological and pharmacological applications.

We have established a biomimetic anti parallel flow architecture and validated its transport behaviour. However, the system remains a single-unit prototype and is not designed for higher throughput studies. The fabrication workflow used in this work supports rapid prototyping, but it does not enable large-scale or high-volume device production. The reliance on full length channel geometry also introduces constraints on throughput because the device operates at a size and layout that favour detailed transport analysis rather than large scale repetition. As a result, although the design performs well within the intended scope of architectural validation, it is not yet suitable for drug screening applications that require multiplexed or repeated units. These practical limitations define the current boundary of the work. Future work will explore pathways to scale the antiparallel flow design into multiple repeated units that can operate on a single substrate. This includes the development of wafer-scale layouts, common inlet and outlet structures, and arrangements that maintain uniform flow while increasing the number of test positions. Additional work will also examine the integration of automated control systems that support continuous perfusion, imaging, and sampling. These developments will help the device move from a single unit study to a platform suitable for more systematic biological or pharmacological investigations. In the longer term, alternative fabrication approaches using thermoplastic materials may provide a method to produce larger quantities of devices with improved consistency. These directions will form the next stage of the development of the LOC platform.

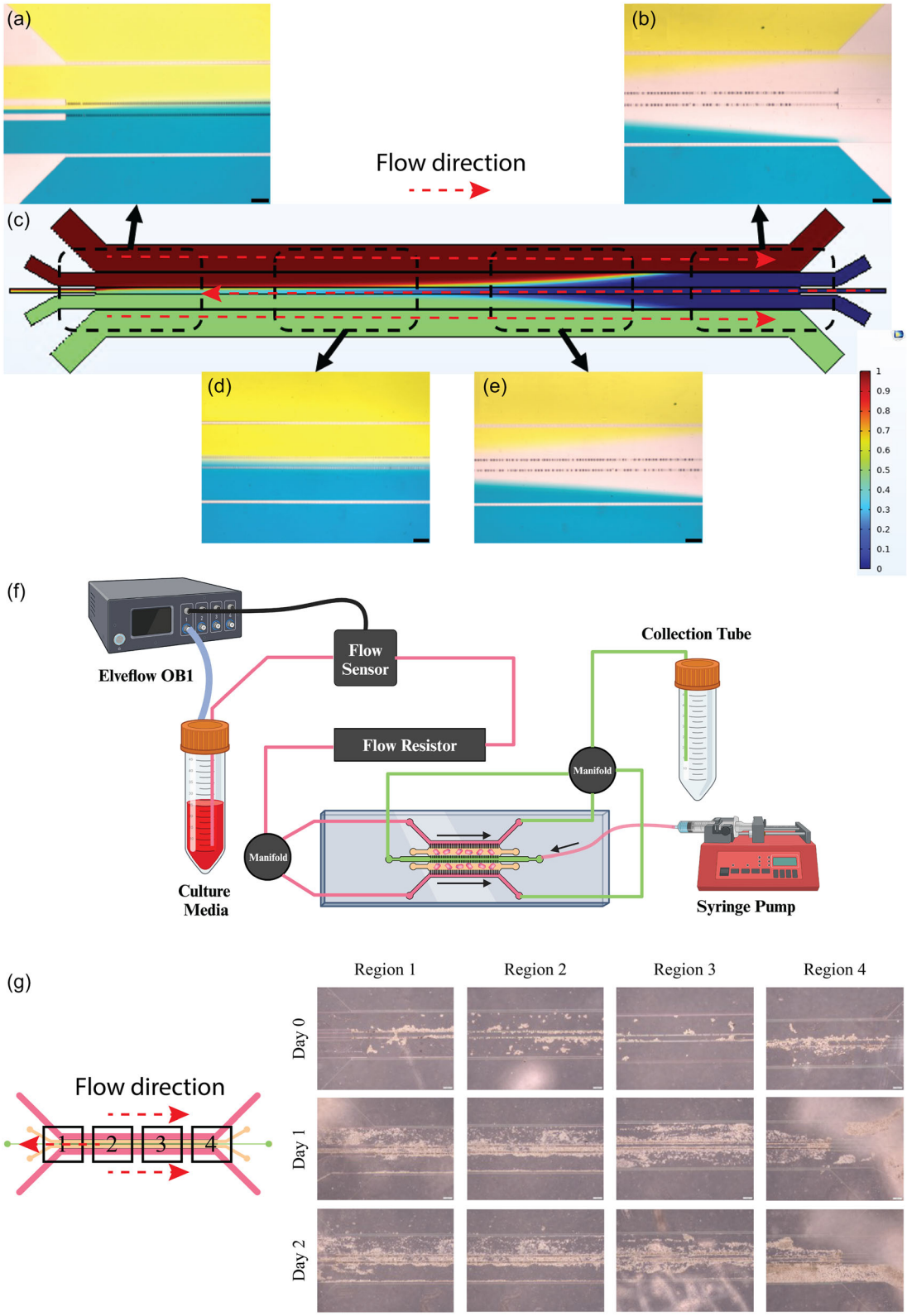

FIGURE 12 | Experimental validation of concentration gradients and cell culture outcomes in the LOC device. (a–e) Experimental visualisation of solute diffusion using blue and yellow food dyes under a media flow rate of 100 μL/min and bile flow rate of 1 μL/min. The distribution of colour closely matches the full-scale simulation results, confirming the length-dependent nature of diffusion in the LOC. (c) Simulated concentration map overlaid with regions corresponding to dye images. (f) Schematic of the experimental flow setup, showing pressure-driven media perfusion via Elveflow OB1 and bile flow controlled by a syringe pump; effluents from both channels were collected in a common tube. (g) Phase contrast images of HepG2 cells in four longitudinal regions of the cell culture channel over a 2-day period. Scale bars = 100 μm.

The present simulations were performed under cell-free conditions because the physical properties of a confluent hepatocyte layer, such as permeability, hydraulic resistance, and surface texture, are not available in a form that allows reliable model construction. Early attempts to include a representative cell layer introduced significant meshing and stability problems and resulted in a large increase in computational load. The aim of the present work is to establish the behaviour of the architectural design at the device scale rather than to resolve microscale interactions at the cell interface. Future studies will include measurements of the physical properties of the cell layer so that these values can be incorporated into refined models that capture the influence of cellular coverage on flow and transport behaviour.

The cell culture results presented in this study are limited to qualitative observations and therefore do not provide a complete assessment of hepatocyte function within the device. This limitation reflects constraints in time and resources that prevented completion of the planned biological evaluation. The present work therefore, focuses on the computational design process and uses the cell study only to demonstrate that the device can support basic culture conditions. Future studies will address this limitation by including a detailed set of quantitative assays that measure cell viability, metabolic activity, and functional outputs such as albumin and urea production. Additional work will examine the development of polarity features and the response of the culture to controlled nutrient conditions within the device. These studies will provide a more complete evaluation of the system and will strengthen the link between the computational design approach and the intended biological application.

3 | Conclusions

In this study, we presented a biomimetic LOC system designed through a computationally guided framework. The principal contribution of this work is the development of a biomimetic design that uses an antiparallel flow arrangement to establish controlled nutrient gradients across the full length of the culture region. This architectural feature defines the function of the device and guides the behaviour observed in the simulations. The computational workflow is used to support this design by allowing evaluation of transport and flow behaviour during the development process. Using COMSOL Multiphysics, we demonstrated that full-scale simulations are essential for accurately capturing diffusion-driven transport phenomena, particularly in microfluidic systems where nutrient and solute delivery is governed by passive mechanisms. Our results reveal that truncated models, while computationally efficient, may introduce significant deviations due to scale-dependent diffusion effects. This finding highlights a critical consideration for future researchers when simplifying geometries in predictive modelling.

The fabricated LOC was experimentally validated and successfully reproduced low-shear, physiologically relevant flow conditions that support hepatocyte viability. Its modular design enables precise control over both flow and concentration gradients, making it well-suited for studies involving gradient-driven responses such as drug dosing, metabolic zonation, and nanoparticle–cell interactions.

Overall, this work underscores the importance of coupling high-fidelity simulations with empirical validation to accelerate the development of organ-on-a-chip systems. By reducing reliance on trial-and-error and ensuring physiologically relevant microenvironments, this integrated approach advances the utility of LOC platforms in biomedical research and preclinical applications.

4 | Materials and Methods

4.1 | COMSOL Simulation

Fluid dynamics were simulated using COMSOL Multiphysics (version 6.2, COMSOL Inc., USA). The simulations used the Laminar Flow physics interface coupled with the Transport of Diluted Species module to solve the steady-state Navier–Stokes and convection–diffusion equations, respectively. Fluid was modelled as Newtonian, with physical properties corresponding to water at 25°C (density: 1000 kg/m^3; dynamic viscosity: 1 mPa·s; diffusion coefficient: 1×10^{-9} m^2/s for the solute). Boundary conditions included a fully developed laminar velocity profile at the inlet (0.1 μL/min, 1 μL/min, 10 μL/min, and 100 μL/min), zero-gauge pressure at the outlet, and no-slip conditions at all solid boundaries. A structured physics-controlled mesh was applied, with local refinement near walls and pillar surfaces to capture shear gradients accurately. Postprocessing included the extraction of velocity fields, pressure profiles, wall shear stress (WSS), and solute concentration distributions. Quantitative comparisons of concentration profiles and shear stress gradients were made across geometries to assess their potential influence on cellular microenvironments.

4.2 | Device Fabrication

The SU-8 master mould was fabricated by ANFF-SA node. Briefly, the master underwent a two-layer photolithography process to define multiscale channel features for subsequent PDMS casting. The fabrication process followed the sequential steps. Silicon wafers were used as substrates. Prior to lithography, the substrates were thoroughly cleaned using a standard cleaning protocol to remove organic and particulate contaminants. Surface treatment, such as dehydration baking, was performed to improve photoresist adhesion. A thin layer of SU-8 photoresist was spin-coated to achieve a thickness of ≈2 μm, targeting fine microchannel structures. The coated substrate underwent soft baking, followed by UV exposure through a high-resolution photomask using a mask aligner, MLA. Post-exposure baking and development were performed according to the SU-8 manufacturer's specifications to form the initial channel layer. Following development, a primer layer was uniformly applied over the developed surface to enhance bonding between the first and second SU-8 layers. The substrate was soft-baked to remove residual solvent. A thicker SU-8 layer (35 μm) was spin-coated onto the primed surface to form the upper channel layer. Alignment was carefully performed to overlay this pattern precisely over the first layer. The fabricated master was inspected under an optical microscope and a surface profilometer to verify the lateral dimensions and feature depths of both layers. Alignment fidelity and structural integrity were also assessed. To facilitate demolding of PDMS replicas, the master mould was vapour-treated with hexamethyldisilazane (HMDS) in a desiccator.

4.3 | Characterisation of Concentration Distribution

The microfluidic chip was fabricated using standard soft lithography process. Briefly, polydimethylsiloxane (PDMS) was mixed thoroughly in a 10:1 ratio of silicone elastomer to the curing agent and was degassed in a desiccator. The degassed mixture was then poured onto the master mould and kept on a hot plate at 60°C for 3 hr for curing. For inlets and outlets, holes were punched using biopsy puncher (150 mm in diameter) on the cured PDMS. The final PDMS pattern was bonded to a glass slide using plasma treatment (Harrick Plasma Basic Plasma Cleaner 115V). Post plasma treatment, the device was placed in an oven for 2 hr to enhance the plasma bonding.

For the visualisation of concentration distribution, blue and yellow coloured food dyes were used. The flow rates were controlled by Harvard Apparatus syringe pump at 100 μL/min. The bile channel was supplied with water and kept at 0.1 μL/min for the duration of the experiment. The chip was imaged using an optical microscope.

4.4 | Cell Culture and Reagents

The cell line HepG2 was gifted from Dr Nichola Calvani from the Sydney School of Veterinary Science at the University of Sydney. The cells were cultured in DEME with 1% (v/v) penicillin-streptomycin and 10% (v/v) FBS. Cells were maintained in 5% CO2 humidified incubator at 37ºC. During subculture, cells were detached by trypsinization when they reached 80% confluency.

4.5 | Microfluidic Operation

HepG2 cells were cultured under continuous perfusion within a LOC platform designed to mimic the antiparallel flow characteristic of liver sinusoids, facilitating efficient nutrient delivery and waste removal. Prior to cell seeding, microfluidic devices were sterilised by exposure to ultraviolet (UV) light for 20 min, followed by flushing with 70% ethanol. Subsequently, the channels were rinsed thoroughly with sterile phosphate-buffered saline (PBS) to eliminate residual ethanol. To promote cell adhesion, a 0.1% gelatin solution was introduced into the channels and incubated at 37°C with 5% CO_2 for 30 min. A 20 μL suspension of HepG2 cells at a concentration of 1.0×10^6 cells/mL (equating to 2.0×10^4 cells per chip) was carefully introduced into the designated cell culture regions via the two cell channels. The devices were then incubated under standard culture conditions (37°C, 5% CO_2) for 2 h to facilitate cell attachment.

Post-attachment, continuous perfusion was initiated using the Elveflow OB1 MK4 pressure controller, renowned for its high precision and rapid response times. The OB1 system was configured with pressurised reservoirs connected to the media inlets of the LOC. A flow rate of 10 μL/min of complete culture medium (DMEM supplemented with 10% fetal bovine serum and 1% penicillin–streptomycin) was maintained through the primary channel. Concurrently, the bile channel was perfused with DMEM at a flow rate of 0.1 μL/min using a Harvard Apparatus syringe pump. To ensure stable and pulseless flow, the OB1 system was operated in flow rate control mode, utilising an integrated flow sensor (e.g., Elveflow MFS series) for real-time feedback. The Elveflow Smart Interface software facilitated the setup and allowed for the implementation of a proportional-integral-derivative (PID) control loop, ensuring precise flow regulation. The microfluidic devices were housed within sterile 150 mm Petri dishes and maintained in a standard cell culture incubator (37°C, 5% CO_2). Fresh culture medium was replenished daily. Cell morphology and proliferation were monitored daily for up to 2 days using phase-contrast microscopy.

Acknowledgments

This research was supported by the Australia–India Strategic Research Fund (Project ID: AIRXIV000039). This work used the NCRIS and Government of South Australia enabled Australian National Fabrication Facility – South Australian Node (ANFF-SA). The authors acknowledge Dr Nichola Eliza Davies Calvani and Dr Katharine Muscat from the Sydney School of Veterinary Science for gifting the HepG2 cell line, with support from the Australian Research Council Discovery Early Career Researcher Award (DECRA; Project ID: DE240100295). Z. Y. acknowledges financial support from the Faculty of Engineering Research Scholarship at the University of Sydney and the University of Sydney Nano Institute Student Ambassador Scholarship.

Open access publishing facilitated by The University of Sydney, as part of the Wiley - The University of Sydney agreement via the Council of Australian University Librarians.

Funding

This work was supported by Australian Government Department of Industry, Science and Resources (DISR) (Grant AIRXIV000039).

Conflicts of Interest

The authors declare no conflicts of interest.

Data Availability Statement

The data that support the findings of this study are available from the corresponding author upon reasonable request.

References

1. C. M. Leung, P. de Haan, K. Ronaldson-Bouchard, et al., "A Guide to the Organ-on-a-Chip," *Nature Reviews Methods Primers* 2 (2022): 33.

2. S. K. Srivastava, G. W. Foo, N. Aggarwal, and M. W. Chang, "Organ-on-Chip Technology: Opportunities and Challenges," *Biotechnology Notes* 5 (2024): 8.

3. D. E. Ingber, "Human Organs-on-Chips for Disease Modelling, Drug Development, and Personalized Medicine," *Nature Reviews Genetics* 23 (2022): 467.

4. S. Deguchi and K. Takayama, "State-of-the-Art Liver Disease Research Using Liver-on-a-Chip," *Inflammation and Regeneration* 42 (2022): 62.

5. Z. Yang, X. Liu, E. M. Cribbin, A. M. Kim, J. J. Li, and K.-T. Yong, "Liver-on-a-Chip: Considerations, Advances, and Beyond," *Biomicrofluidics* 16 (2022), https://doi.org/10.1063/5.0106855.

6. S. Hassan, S. Sebastian, S. Maharjan, et al., "Liver-on-a-Chip Models of Fatty Liver Disease," *Hepatology* 71 (2020): 733.

7. A. Ehrlich, D. Duche, G. Ouedraogo, and Y. Nahmias, "Challenges and Opportunities in the Design of Liver-on-Chip Microdevices," *Annual Review of Biomedical Engineering* 21 (2019): 219.

8. S. Li, C. Li, M. I. Khan, et al., "Microneedle Array Facilitates Hepatic Sinusoid Construction in a Large-Scale Liver-Acinus-Chip Microsystem," *Microsystems & Nanoengineering* 9 (2023): 75.

9. V. Carvalho, M. Ferreira, R. O. Rodrigues, S. F. C. F. Teixeira, and R. A. Lima, "Computational and Experimental Advances in Liver-on-a-Chip Technology for Cancer Research: A Systematic Review," *Biophysical Reviews* 17 (2025): 151.

10. M. K. Kim, K. Paek, K. Park, et al., "A Hepatic Zonation Chip with an Oxygen Concentration Gradient Embracing the Spatial Distribution of Metabolic Function," *Biofabrication* 17 (2025): 035019.

11. J. Kassis and Z. Wan, "Latest Advancements in Organ-on-a-Chip Technology," *Frontiers in Pharmacology* 16 (2025): 1631320, https://doi.org/10.3389/fphar.2025.1631320.

12. H. Liu, X. Zhang, Y. Wang, et al., "Standard: Human Liver-on-a-Chip," *Cell Regeneration* 14 (2025): 9.

13. H. Rashidi, S. Alhaque, D. Szkolnicka, O. Flint, and D. C. Hay, "Fluid Shear Stress Modulation of Hepatocyte-Like Cell Function," *Archives of Toxicology* 90 (2016): 1757.

14. W. Li, Y. Wu, W. Hu, et al., "Direct Mechanical Exposure Initiates Hepatocyte Proliferation," *JHEP Reports* 5 (2023): 100905.

15. S. Y. Lee, D. Kim, S. H. Lee, and J. H. Sung, "Microtechnology-Based In Vitro Models: Mimicking Liver Function and Pathophysiology," *APL Bioengineering* 5 (2021), https://doi.org/10.1063/5.0061896.

16. M. Gori, M. C. Simonelli, S. M. Giannitelli, L. Businaro, M. Trombetta, and A. Rainer, "Investigating Nonalcoholic Fatty Liver Disease in a Liver-on-a-Chip Microfluidic Device," *PLoS One* 11 (2016): e0159729.

17. X. Ma, X. Qu, W. Zhu, et al., *Proceedings of the National Academy of Sciences* 113 (2016): 2206.

18. N. Filipovic, M. Nikolic, and T. Sustersic, *Biomaterials for Organ and Tissue Regeneration* (Elsevier, 2020), 753–790.

19. Y. Wang, L. Marucci, and M. E. Homer, "In Silico Modelling of Organ-on-a-Chip Devices: An Overview," *Frontiers in Bioengineering and Biotechnology* 12 (2025): 1520795, https://doi.org/10.3389/fbioe.2024.1520795.

20. F. Pisapia, W. Balachandran, and M. Rasekh, "Organ-on-a-Chip: Design and Simulation of Various Microfluidic Channel Geometries for the Influence of Fluid Dynamic Parameters," *Applied Sciences* 12 (2022): 3829.

21. C. Decaens, M. Durand, B. Grosse, and D. Cassio, *Biology of the Cell* 100 (2008): 387.

22. P. Gissen, and I. M. Arias, "Structural and Functional Hepatocyte Polarity and Liver Disease," *Journal of Hepatology* 63 (2015): 1023.

23. Y. Song, D. Cheng, and L. Zhao, *Microfluidics: Fundamental, Devices and Applications* (Wiley, 2018).

24. K. Kaarj and J.-Y. Yoon, "Methods of Delivering Mechanical Stimuli to Organ-on-a-Chip," *Micromachines* 10 (2019): 700.

25. W. E. Svendsen, *Lab-on-a-Chip Devices and Micro-Total Analysis Systems* (Springer International Publishing, 2015), 17–26.

26. A. Dietzel, *Microsystems for Pharmatechnology* (Springer International Publishing, 2016), 1–21.